Nano Energy (▮▮▮▮) ▮, ▮▮▮–▮▮▮

Available online at www.sciencedirect.com

ScienceDirect

journal homepage: www.elsevier.com/locate/nanoenergy

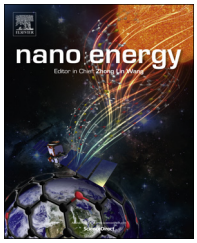

RAPID COMMUNICATION

Ultrasensitive self-powered cytosensor

Pan-Pan Gai[a], Yu-Sheng Ji[a], Wen-Jing Wang[a], Rong-Bin Song[a], Cheng Zhu[a], Yun Chen[a], Jian-Rong Zhang[a,b,*], Jun-Jie Zhu[a,*]

[a]*State Key Laboratory of Analytical Chemistry for Life Science, School of Chemistry and Chemical Engineering, Nanjing University, Nanjing 210093, PR China*
[b]*School of Chemistry and Life Science, Nanjing University Jinling College, Nanjing 210089, PR China*

Received 30 December 2014; received in revised form 3 March 2015; accepted 26 March 2015

KEYWORDS
Self-powered cytosensor;
Biofuel cells;
Acute leukemia CCRF-CEM cells

Abstract
We developed an ultrasensitive self-powered cytosensor based on biofuel cells (BFC) for the detection of acute leukemia CCRF-CEM cells. The core component of the BFC cytosensor was composed of an aptamer (Sgc8c)-functionalized cathode and a nitrogen-doped graphene/gold nanoparticles/glucose oxidase (NG/AuNPs/GOD) anode, which generated a maximum power output density (P_{max}) of 115 μW cm^{-2}. Once the negatively charged CCRF-CEM cells were captured by the cathode *via* aptamer recognition, their dramatic steric hindrance and electrostatic repulsion to the redox probe $[Fe(CN)_6]^{3-}$ efficiently blocked the electron transfer between the probe and the cathode surface, and thereby caused a remarkable decrease in power output of the BFC, which could be used to sensitively detect the cells. Notably, the power output density of the BFC cytosensor could be restored when the captured CCRF-CEM cells were released from the aptamer-functionalized cathode by raising the temperature of the cathode to alter the specific conformation of the aptamer. Then the re-activated cathode could capture CCRF-CEM cells once again achieving the regeneration of the BFC cytosensor. This self-powered BFC cytosensor showed a linear relationship between the P_{max} and the logarithm of the cell numbers over a range of 5–50,000 cells (r=0.9979) with a detection limit of 4 cells (S/N=3), which is expected to have potential application as a powerful point-of-care tool for the early detection of circulating tumor cells.

Introduction

Biofuel cells (BFC) have attracted considerable interest recently because of their ability to provide sustainable energy from renewable fuel sources in mild conditions

*Corresponding authors at: State Key Laboratory of Analytical Chemistry for Life Science, School of Chemistry and Chemical Engineering, Nanjing University, Nanjing 210093, PR China.
E-mail addresses: jrzhang@nju.edu.cn (J.-R. Zhang), jjzhu@nju.edu.cn (J.-J. Zhu).

http://dx.doi.org/10.1016/j.nanoen.2015.03.035
2211-2855/

[1,2]. As an efficient energy conversion technology, the development of BFC has not only been confined in employing novel materials to improve the cell performance [3-6], but also constructing new devices to expand their potential applications, *i.e.*, power extracting from living creatures [7-9], and miniaturization for low-cost, portable power devices [10,11]. Self-powered sensors based on BFC, one kind of biofuel cells with power output as an analytical signal that is proportional to the analyte concentration [12], have been developed for various applications including the determination of biomolecule [12-15], toxic pollutant [16-18] and immunization analysis [19-21]. The unique characteristics of the self-powered sensors, such as no need for external power sources, simple fabrication process, miniature size and low cost [22-26], make them as promising candidates in human disease diagnosis.

Leukemia is a type of fatal cancer that affects the bone marrow, the blood cells, and other parts of the lymphatic system [27]. According to the study conducted by American Cancer Society, there are about 20,660 new cases of leukemia in the United States in 2013, leading to a poor survival rate of less than 50% [28]. More seriously, leukemia has complicated etiology and pathogenesis, which makes it difficult to select suitable treatment options to the specific symptom of the disease [29]. However, early detection of leukemia, especially acute leukemia, could make the treatment more effective and improve the cure rates. Therefore, it is imperative to develop a sensitive and reliable appraisal system for early diagnosis, classification and prognosis of acute leukemia. To date, a variety of tools have been applied in acute leukemia diagnosis, such as the complete blood count and peripheral blood smear [30], immunophenotyping by flow cytometry [31] or microarrays [32], and polymerase chain reaction (PCR)-based DNA tests [33]. These methods suffer from either time-consuming sample preparation procedures or sophisticated instrumentation, which limits their use as point-of-care diagnostic tools. In addition, the amplification of malignant cell mutations by even PCR may lead to false-negative results in some cases [34]. Thus, there is an urgent need to develop a robust preliminary testing approach, which can provide more accurate and quantitative diagnostic results in a timely manner for the early detection of acute leukemia. Recently, we have developed a series of electrochemical cytosensors toward the detection of acute leukemia [28,35]. However, the potential applied on the electrode may cause some nonspecific redox of the electroactive interferences.

Herein, using CCRF-CEM cells as representative leukemia model, we fabricated an ultrasensitive self-powered BFC cytosensor, in which the cell concentration was proportional to the power output signal of BFC. As shown in Scheme 1A, the aptamer Sgc8c, which could specifically and efficiently recognize the protein tyrosine kinase 7 (PTK7) overexpressed on CCRF-CEM cells [36], was functionalized on the gold electrode that served as the cathode of the BFC for recognizing CCRF-CEM cells; while the nitrogen-doped graphene/gold nanoparticles/glucose oxidase (NG/AuNPs/GOD) composite modified carbon paper was used as the anode to oxidize glucose. In the absence of CCRF-CEM cells, the electrons produced by glucose oxidization were transferred to cathode, leading to the reduction of the $[Fe(CN)_6]^{3-}$ probe, and the power output of BFC was measured. Once the target cells were captured by the cathode *via* aptamer recognition, their dramatic steric hindrance would greatly block the electron transfer between $[Fe(CN)_6]^{3-}$ and cathode surface (Scheme 1B). Moreover, the electrostatic repulsion between the negatively charged cells and high valent anion $[Fe(CN)_6]^{3-}$ further inhibited the electron transfer of the probe [37], which caused a remarkable decrease in power output of the BFC. In this case, we could detect the CCRF-CEM cells only by measuring the change of power output signal of BFC without needing external power source. Furthermore, only in specific 3D conformation could the aptamer recognize the target protein on cell membrane, and thus altering its conformation would release the captured CCRF-CEM cells from the cathode, which could be realized by a moderate temperature change of the cathode to reversibly disrupt the aptamer-cell interaction [38], resulting in the regeneration of the cathode interface and reutilization of the cytosensor. This novel strategy for the fabrication of ultrasensitive self-powered cytosensor was proven to be effective, which is expected to have great potential application as a powerful point-of-care tool for early diagnosis of cancer.

Experimental section

Materials and chemicals

Thiolated aptamers synthesized and purified by Shanghai Sangon Biotechnology Co. Ltd. (Shanghai, China). The sequence of the thiolated-Sgc8c aptamer (SH-Sgc8c) was 5′-HS-ATC TAA CTG CTG CGC CGC CGG GAA AAT ACT GTA CGG TTA GA-3′. Glucose oxidase (GOD) from *Aspergillus niger* (EC 1.1.3.4, 158.9 units mg^{-1}), 1-ethyl-3-(3-dimethylaminopropyl) carbodiimide hydrochloride (EDC), *N*-hydroxysuccinimide (NHS), Tris (2-carboxyethyl) phosphine hydrochloride (TCEP), calcein acetoxymethyl ester (calcein-AM), 6-mercapto-1-hexanol (MCH) and Dulbecco's phosphate-buffer saline (D-PBS) with $CaCl_2$ and $MgCl_2$ were all purchased from Sigma-Aldrich (St. Louis, USA). All reagents were of analytical grade and were used without further purification. Ultra-pure water (18.2 MΩ resistivity, Milli-Q, Millipore) was used for all the experiments.

Apparatus

Confocal laser scanning microscopy (CLSM) studies were performed using a Leica TCS SP5 fluorescence microscope (Germany). Electrochemical impedance spectroscopy (EIS) was carried on an Autolab electrochemical analyzer (Eco Chemie, The Netherlands) within a frequency range of 0.1 Hz to 100 kHz. 2.5 mM $K_3Fe(CN)_6/K_4Fe(CN)_6$ was used as probe and 0.5 M KNO_3 dissolved in D-PBS (pH 7.4) with $CaCl_2$ and $MgCl_2$ was used as the supporting electrolyte. The measurements of both cyclic voltammetry (CV) and linear sweep voltammetry (LSV) were performed on a CHI 660B electrochemical workstation (CH Instruments, Shanghai) using a three-electrode system: the fabricated cathode or anode as the working electrode, Pt wire as the counter-electrode, and an SCE as the reference electrode.

Please cite this article as: P.-P. Gai, et al., Ultrasensitive self-powered cytosensor, Nano Energy (2015), http://dx.doi.org/10.1016/j.nanoen.2015.03.035

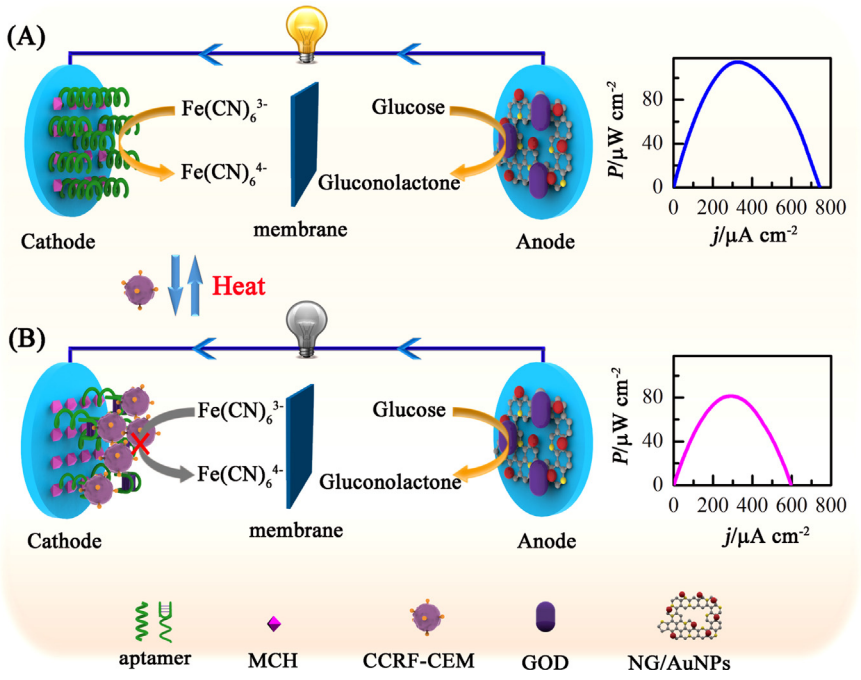

Scheme 1 Schematic illustration of the self-powered BFC cytosensor.

Cell lines and cell culture

CCRF-CEM cells were obtained from Nanjing Key Gen Biotech Co., Ltd. and cultured in a flask in RPMI 1640 medium (Gibco, Grand Island, NY) supplemented with 10% fetal calf serum (FCS, Sigma), penicillin (100 μg mL^{-1}) and streptomycin (100 μg mL^{-1}) in an incubator (5% CO_2, 37 °C). At the logarithmic growth phase, the cells were collected and separated from the medium by centrifugation at 1000 rpm for 2 min and then suspended in the binding buffer (both 4.5 g L^{-1} glucose and 5 mM $MgCl_2$ dissolved in D-PBS with $CaCl_2$ and $MgCl_2$) to obtain a homogeneous cell suspension. The binding buffer was used to ensure the effective binding affinity between cells and aptamers [39].

Fabrication and measurement of the BFC cytosensor

A gold disk electrode with a diameter of 4.0 mm was used as a substrate cathode. Prior to use, the gold disk electrode was polished successively with 1.0, 0.3, and 0.05 μm alumina powders, sonicated successively in ethanol and ultrapure water, and dried with flowing N_2 gas. The polished gold electrode was treated with piranha solution (98% H_2SO_4+30% H_2O_2 (v/v 3:1)) for 5 min to remove possible surface contamination. The treated gold electrode was reversibly cycled in a 0.5 M H_2SO_4 solution from 0 to 1.8 V (*vs* SCE) until an ideal redox wave of H_2SO_4 was observed, and then the electrode was rinsed with H_2O and dried with flowing N_2 gas. 10 μL of SH-Sgc8c (1.0 μM) aptamer was immediately applied to the treated gold electrode and incubated at 4 °C overnight. SH-Sgc8c aptamer was assembled onto the gold electrode surface through Au-S bond. After the aptamer-functionalized gold electrode was rinsed with ultrapure water, 20 μL of 1 mM MCH was dropped on the surface of the aptamer-functionalized gold electrode and incubated for 1 h at room temperature to block the nonspecific binding sites, and then washed with ultrapure water thoroughly. The fabricated aptamer-functionalized cathode was placed in the cathode chamber containing 20 mM $K_3Fe(CN)_6$ probe dissolved in D-PBS (pH 7.4) with $CaCl_2$ and $MgCl_2$.

The anode of the BFC was fabricated as follows, 100 μL of as-prepared NG/AuNPs suspension reported previously in our group was dropped on the surface of carbon paper electrode (1 cm × 1 cm) [40]. After drying for 2 h at 37 °C, the NG/AuNPs electrode was immersed into a solution containing 1 mg mL^{-1} EDC and NHS for 30 min to activate the carboxyl group on the NG/AuNPs surface. After rinsing with ultrapure water to get rid of the excess EDC and NHS, the activated NG/AuNPs electrodes were immersed into 1 mL of GOD solution (50 mg mL^{-1}, dissolved in pH=9.0 Tris-HCl) for 24 h at 4 °C. GOD was bound to the NG/AuNPs electrode through a condensation reaction between terminal amino groups on lysine residues of GOD and carboxyl groups on the AuNPs [40]. The fabricated anode was placed in anode chamber containing 50 mM glucose dissolved in 0.1 M PBS (pH=7.4) saturated with nitrogen.

The anodic and cathodic chamber of the BFC cytosensor was separated by perfluorosulfonic acid/PTFE copolymer membrane (DuPont™ Nafion® PFSA NRE-211, 25.4 μm).

For cytosensing, the aptamer-modified cathode was first soaked in 50 μL of target cell suspension at a certain concentration and incubated at 4 °C for 30 min to capture the cells. After the electrode was taken out and rinsed with incubation buffer to remove the non-captured cells carefully, it was put back into the cathode chamber, and the power output of BFC cytosensor was measured.

In order to regenerate the detection of the cytosensor, the cell-captured cathode was taken out from the cathode chamber and incubated in 48 °C D-PBS for 10 min, which

Please cite this article as: P.-P. Gai, et al., Ultrasensitive self-powered cytosensor, Nano Energy (2015), http://dx.doi.org/10.1016/j.nanoen.2015.03.035

could release the captured cells and re-activate the cathode. Then the measurement followed the same cell captured steps as above.

Polarization curves of the BFC cytosensor were measured by LSV starting from the open-circuit value at a scan rate of 1 mV s^{-1}. The relationship of power output and current was calculated based on the polarization curve by the formula of $P=UI$. The results were normalized to the projective surface area of the cathode (0.1256 cm^2).

Results and discussions

Characterization of the cathode

The immobilization of the aptamer and the recognition of the target cells on cathode were monitored by cyclic voltammograms (CVs) using the redox probe of $Fe(CN)_6^{3-}$. As shown in Figure 1A, a pair of well-defined redox peaks of $Fe(CN)_6^{3-/4-}$ were observed at the bare gold electrode (curve a). After the bare gold electrode was self-assembled with thiol-terminated aptamer (Sgc8c), the peak-to-peak potential separation increased as well as the peak current decreased (curve b), ascribing to the electrostatic repulsion between the negatively charged aptamer and $[Fe(CN)_6]^{3-}$. The increased irreversibility of the interfacial electron transfer indicated the successful assembly of the aptamer. Afterwards, MCH was used to block the nonspecific binding sites on the electrode. Due to its non-conductivity, the resistance of the interfacial electron transfer was further increased with a continuous decrease of the peak current. Upon the binding of CCRF-CEM cells onto the aptamer-functionalized electrode, a remarkable decrease in the cathodic peak current from 76.39 to 44.2 μA was observed, which was attributed to the fact that the CCRF-CEM cells bound to the cathode would bring a dramatic steric hindrance to the electron transfer of $[Fe(CN)_6]^{3-}$ probe, while the electrostatic repulsion between the negatively charged cells and $[Fe(CN)_6]^{3-}$ further increased the resistance of electron transfer [37]. Those results demonstrated that the aptamer-functionalized cathode had successfully captured the target cells.

Furthermore, the recognition of the modified cathode to the CCRF-CEM cells was also confirmed by EIS measurements. The electron-transfer resistance (R_{et}) of the redox probe, $[Fe(CN)_6]^{3-}/[Fe(CN)_6]^{4-}$, was measured during the cathode assembly process and the resulting Nyquist plots are shown in Figure 1B. The EIS results were fitted to a Randles equivalent circuit (inset in Figure 1B), which consisted of the solution resistance (R_s), R_{et} of $[Fe(CN)_6]^{3-}/[Fe(CN)_6]^{4-}$, the constant phase element (C_{dl}) and Warburg impedance (W). In the Nyquist diagrams, the diameters of the semicircles reflected the R_{et} of $[Fe(CN)_6]^{3-}/[Fe(CN)_6]^{4-}$ on the cathode at certain applied potentials. It was observed from Figure 1B that the R_{et} of the probe significantly increased after the cathode was modified by Sgc8c aptamer and blocked with MCH because the modified molecules might form an inert blocking layer to hinder the electron transfer. The subsequent capture of the CCRF-CEM cells

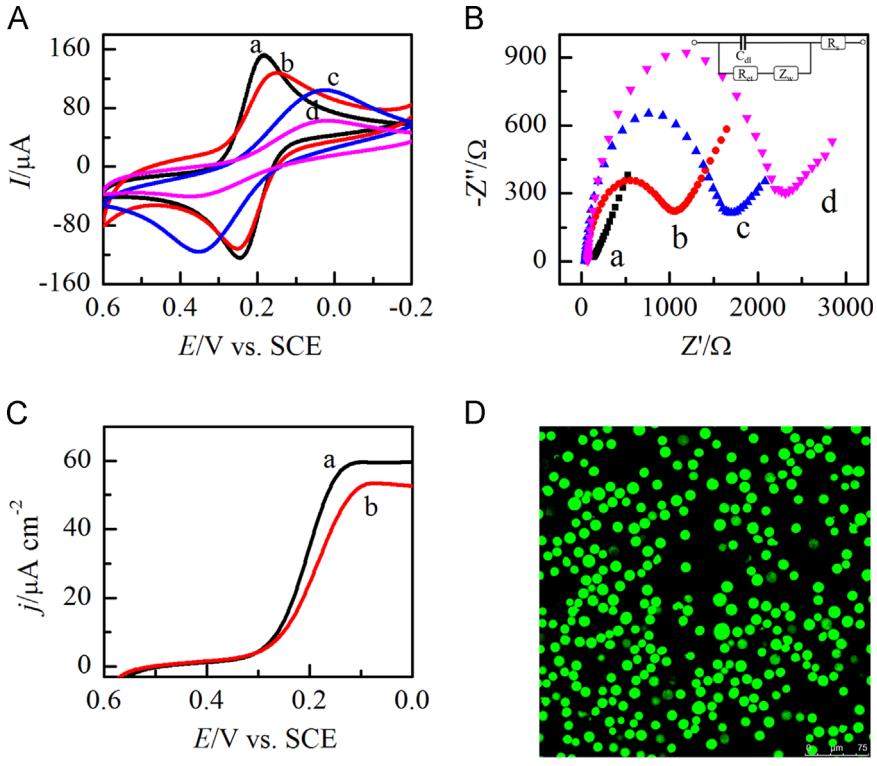

Figure 1 (A) CVs of the bare gold electrode (a), the Sgc8c-modified electrode (b), the Sgc8c-MCH-modified electrode (c), and the Sgc8c-MCH-modified electrode incubated in 5000 cell suspension (d). (B) EIS of the bare gold electrode (a), the Sgc8c-modified electrode (b), the Sgc8c-MCH-modified electrode (c), and the Sgc8c-MCH-modified electrode incubated in 5000 cell suspension (d). (C) Polarization curves of the cathode before (a) and after (b) incubated in 5000 cell suspension. (D) Fluorescence microscopy image of CCRF-CEM cells stained with calcein-AM after they were captured on the cathode surface.

Please cite this article as: P.-P. Gai, et al., Ultrasensitive self-powered cytosensor, Nano Energy (2015), http://dx.doi.org/10.1016/j.nanoen.2015.03.035

onto the Sgc8c-MCH-modified cathode further obstructed the access of the redox probes to the cathode surface due to the steric hindrance effect and electrostatic repulsion of the negative cells to anion probe, showing as an elevated R_{et} (curve d in Figure 1B). Additionally, the polarization curves of the cathode are recorded before and after the cells were captured (Figure 1C). In the absence of CCRF-CEM cells, the reduction current density of $Fe(CN)_6^{3-}$ at the cathode reached a plateau of 59.97 μA cm^{-2} at +0.1 V. After the cathode was incubated in the CCRF-CEM cell suspension, the plateau of the reduction current density decreased to 53.74 μA cm^{-2} at +0.088 V, which further demonstrated the successful capture of the target cells.

Furthermore, to visualize the cell viability, we stained the captured cells with calcein-AM, a widely used cell viability indicator that only stained living cells. The strong fluorescence signals from the cells on the cathode surface (Figure 1D) indicated that the cells were alive during the whole sensing process.

Regeneration of the cathode

The tertiary structures of aptamers have directly determined their binding efficiency to the molecular targets [41]. That is, only the specific 3D conformation could facilitate Sgc8c to interact with the membrane protein PTK7, and thus altering the conformation of aptamer by changing temperature could release the captured cells [42], further resulting in the regeneration of the cathode interface. This cathode switch processes were monitored by CVs and EIS measurements (Figure 2). In the absence of CCRF-CEM cells, the reduction current of $Fe(CN)_6^{3-}$ probe was measured as 76.06 μA at the cathode (a in Figure 2A and B), while the current significantly reduced to 46.34 μA after the CCRF-CEM cells were captured (b in Figure 2A and B). Then the cathode was incubated in 48 °C D-PBS for 10 min, the probe current was rapidly restored to 79.39 μA (c in Figure 2A and B), indicating the successful release of the captured cells from the electrode surface and re-activation of the cathode [38]. Subsequently, the re-activated cathode was incubated in CCRF-CEM cell suspension at 4 °C for 30 min, and the probe current of the cathode reduced to 48.86 μA again (d in Figure 2A and B), suggesting that the CCRF-CEM cells had been successfully captured by the re-activated cathode. Furthermore, Figure 2C and D showed that the R_{et} of the probe at the cathode (a in Figure 2C and D) and re-activated cathode (c in Figure 2C and D) was approximate equivalent, and after incubated with CCRF-CEM cells, the re-activated cathode has an increasing R_{et} value (d in Figure 2C and D), which all demonstrated the cathode has been regenerated and could successfully recognize CCRF-CEM cells. Due to the conformational reversibility of the aptamer to temperature, the aptamer-functionalized cathode could be used repeatedly.

Characterization of the anode

To examine the immobilization of GOD and the effective oxidation of glucose at the NG/AuNPs/GOD anode, cyclic voltammetry of the NG/AuNPs electrode and NG/AuNPs/GOD electrode were carried out (Figure 3A). Compared to NG/AuNPs electrode, NG/AuNPs/GOD electrode showed a couple of well-defined redox peaks at −0.512 and −0.463 V, respectively, which could be ascribed to the characteristic peaks of GOD [43]. Moreover, both the cathodic and the anodic peaks of GOD were almost symmetrical with respect to the potential axis, indicating that GOD could directly transfer the electron from the active sites of GOD to electrode. Figure 3B shows the polarization of the anode in the absence (curve a) or presence of 50 mM glucose (curve b). The oxidation of glucose at the NG/AuNPs/GOD electrode occurred at a low potential of −0.4 V and the anodic current density reached to 89 μA cm^{-2} at 0.1 V, which suggested the high catalytic ability of NG/AuNPs/GOD anode to glucose oxidation. These results also indicated that the kinetics at the aptamer-functionalized cathode (the cathode current density, 59.97 μA cm^{-2}) was the limiting factor to the power output for the BFC, meaning that the power output signal could be employed to assess the number of the target cell captured by the aptamer-functionalized cathode.

BFC cytosensor for sensing CCRF-CEM cells

Once the CCRF-CEM cells were captured by the aptamer-functionalized cathode, a remarkable decrease in the cathodic peak current (i_{pc}) and an increase in peak-to-peak potential separation (ΔE_p) were observed (Figure 1 and Figure 2), which indicated that the power ($I_{BFC}U_{BFC}$) changes of the BFC were far greater than the current (i_{pc}) changes of a single aptamer cathode. That is, the BFC cytosensor would be more sensitive than the single aptamer cathode for sensing cells. Meantime, no external power sources were needed in the cytosensor construction, which also facilitated the cell detection. Therefore, the aptamer-functionalized cathode coupled with NG/AuNPs/GOD anode was selected to fabricate the BFC cytosensor.

Figure 4A displays the polarization curve and power output curve of the assembled BFC cytosensor with 20 mM $Fe(CN)_6^{3-}$ in cathode chamber and 50 mM glucose in anode chamber. The maximum power output density (P_{max}) and the open potential of the cytosensor reached to 115 μW cm^{-2} and 0.7 V, respectively. Figure 4B and C depicts that both the polarization curves and power output curves were able to distinguish the different numbers of CCRF-CEM cells. The P_{max} of the cytosensor decreased with the increase of cell numbers (N_{cells}), while the calibration curve for the cells displayed a linear relationship between P_{max} and the logarithm of the cell numbers (N_{cells}) over a range of 5–50,000 cells with a correlation coefficient of 0.9979 and a linear equation of $P_{max}=113.01-6.62\log N_{cells}$ (Figure 4D). The limit of detection for CCRF-CEM cells was determined to be 4 cells ($S/N=3$), which was significantly improved compared to other acute leukemia cytosensing approaches based on electrochemical cytosensor (35 cells) [28] and electrochemical impedance spectroscopy (30 cells) [44].

To verify the regeneration of the self-powered cytosensor, three independent cytosensors were fabricated and tested in the same conditions. The cathode of the cytosensor was first introduced to CCRF-CEM cell suspension to capture the target cells, and then put back to the cathode chamber of the cytosensor; P_{max} of the cytosensor was

Please cite this article as: P.-P. Gai, et al., Ultrasensitive self-powered cytosensor, Nano Energy (2015), http://dx.doi.org/10.1016/j.nanoen.2015.03.035

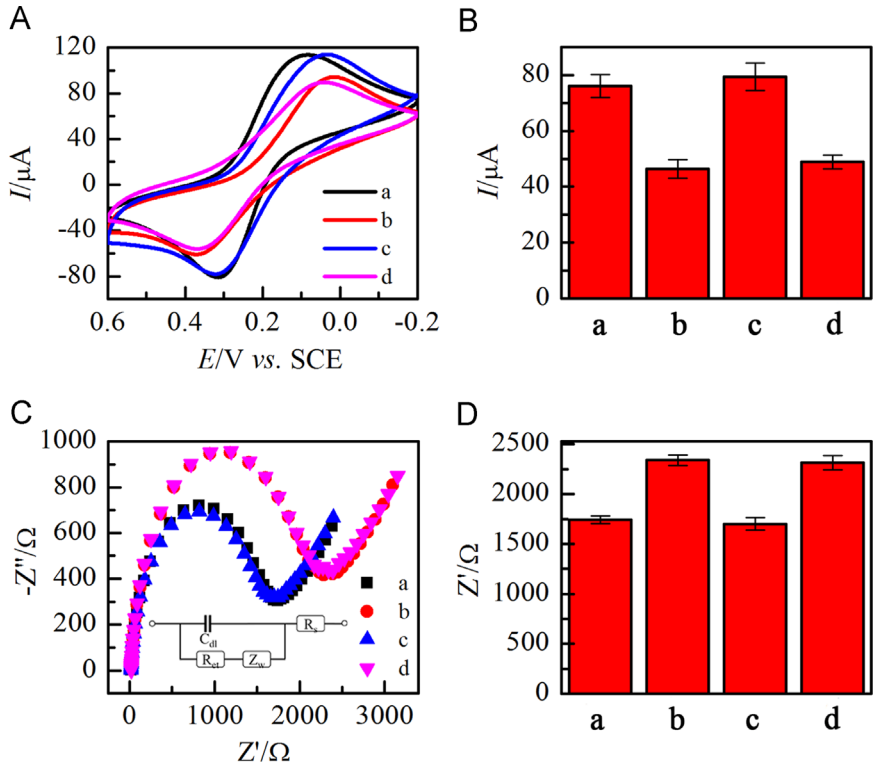

Figure 2 (A) CVs and (B) current histogram of the $Fe(CN)_6^{3-}$ probe at the aptamer-functionalized cathode before (a) and after (b) incubated in 5000 cell suspension and at the re-activated cathode before (c) and after (d) incubated in 5000 cell suspension. υ=100 mV s^{-1}. (C) EIS and (D) R_{et} value of the aptamer-functionalized cathode before (a) and after (b) incubated in 5000 cell suspension and at the re-activated cathode before (c) and after (d) incubated in 5000 cell suspension.

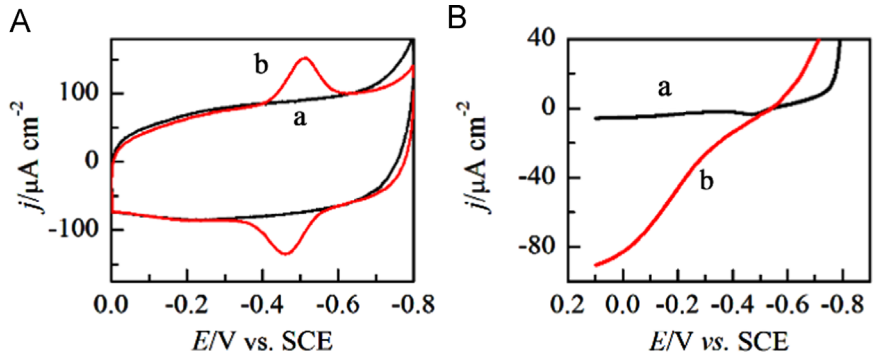

Figure 3 (A) CVs of the NG/AuNPs electrode (a) and NG/AuNPs/GOD electrode (b) in PBS (pH=7.4), υ=10 mV s^{-1}. (B) Polarization curves of the NG/AuNPs/GOD electrode in PBS (pH=7.4) without (a) or with (b) 50 mM glucose, υ=1 mV s^{-1}.

measured (Capture in Figure 5A). Subsequently, the cell-captured cathode was brought out from the cathode chamber and incubated in 48 °C D-PBS for 10 min to release the captured cells and re-activate the cathode, and P_{max} of the cytosensor was measured again (Regenerate in Figure 5A), which was defined as one cycle. For the regenerated cytosensor, the re-activated cathodes followed the same cell captured steps as above, and the obtained P_{max} of the regenerated cytosensor could be used to detect the CCRF-CEM cells. As shown in Figure 5A, in the absence and presence of CCRF-CEM cells, the difference of maximum power output (ΔP_{max}) of the BFC cytosensor was 34 μW cm^{-2} at the first measurement and 22 μW cm^{-2} at the sixth with only 35.2% loss of ΔP_{max}. After the operation of six cycles, the small loss of ΔP_{max} could be attributed to the unavoidable contamination of the substrate [45], such as the nonspecific adsorption of cellular debris or free protein in cell suspension at the cathode, might block the electron transfer between $[Fe(CN)_6]^{3-}$ and cathode surface. All the results clearly demonstrated that the self-powered BFC cytosensor could be utilized repeatedly.

The specificity for the CCRF-CEM cells detection is also a key issue in cytosensing. In this case, HL-60 and K562 cells at 10 times concentration of target cells were selected as negative controls to evaluate the selectivity of the cytosensor. Figure 5B shows that the P_{max} of the cytosensor in the presence of 5000 CCRF-CEM cells (P_1) were compared with those in the presence of 5000 CCRF-CEM cells and

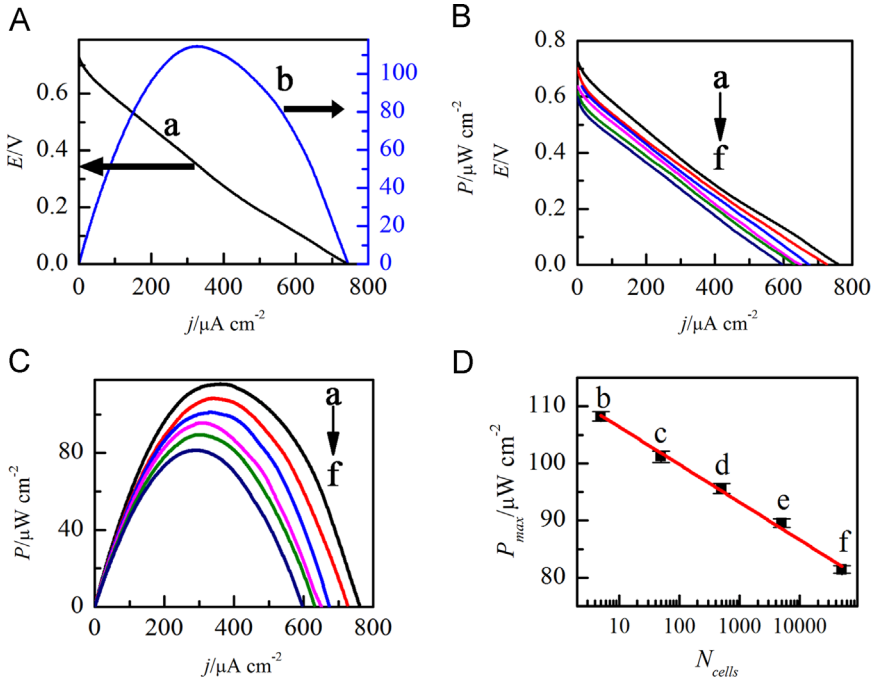

Figure 4 (A) Polarization curve (a) and power output curve (b) of the BFC cytosensor. (B) Polarization curves and (C) power output curves of the cytosensor response to different numbers of CCRF-CEM cells (from curves a to f: 0, 5, 50, 500, 5000, 50,000 cells). (D) The plot of P_{max} *vs* the logarithm of the numbers of CCRF-CEM cells. Error bars represent the standard deviation of an average value from independent measurements of three cytosensors.

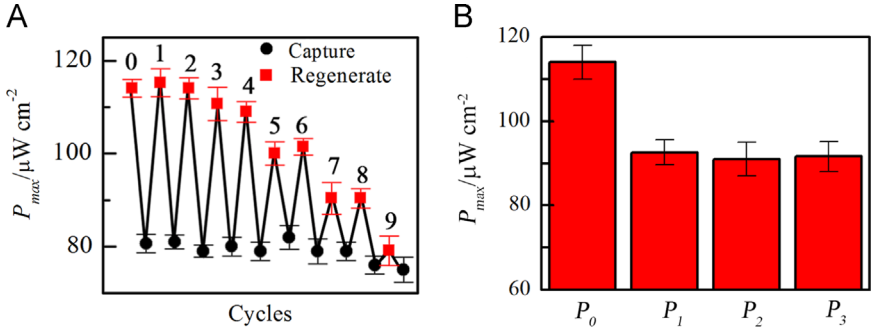

Figure 5 (A) The P_{max} of BFC cytosensor during 9 cycles. Black circle dots (Capture) represent the P_{max} of BFC cytosensor after the cathode was incabuted in 50,000 cell suspension and red square dots (Regenerate) represent the P_{max} of the regenerated BFC cytosensor. Error bars represent the standard deviation of an average value from independent measurements of three cathodes. (B) The histogram of the P_{max} of BFC cytosensor in the absence of cells (P_0) and the P_{max} of the BFC cytosensor in the presence of 5000 CCRF-CEM cells (P_1), 5000 CCRF-CEM cells and 50,000 K562 cells (P_2) or 5000 CCRF-CEM cells and 50,000 HL-60 cells (P_3), respectively. The error bars represent the standard deviation obtained from measurements performed on three cytosensors.

50,000 K562 cells (P_2) or 5000 CCRF-CEM cells and 50,000 HL-60 cells (P_3). It was apparent that the interference of the control cells was neglectable for the detection of target cells due to the high binding specificity and affinity of the aptamer, which demonstrated that the proposed BFC cytosensor had good specificity and was capable of discriminating CCRF-CEM cells from complex samples.

Conclusions

We constructed an ultrasensitive self-powered cytosensor based on BFC for the detection of CCRF-CEM cells. This cytosensor does not need external applied voltage, which efficiently eliminates the nonspecific redox of the electro-active interferences, improves the anti-fouling ability of the cytosensor, and facilitates the sensor miniaturization for *in vivo* application. Meantime, the high binding specificity and affinity of the aptamer, as well as the power output signal of the BFC, make the cytosensor possess excellent selectivity and sensitivity for sensing CCRF-CEM cells, which was superior to other leukemia cytosensing approaches reported previously. Furthermore, the re-activity of the aptamer cathode endows the cytosensor regenerated making cytosensing more practical and the regeneration effect of our cytosensor is proven to be promising in the fabrication of reusable cytosensor in the future. The proposed strategy for fabrication of the cytosensor is expected to become a general consideration in constructing cytosensing platform for human disease detection.

Please cite this article as: P.-P. Gai, et al., Ultrasensitive self-powered cytosensor, Nano Energy (2015), http://dx.doi.org/10.1016/j.nanoen.2015.03.035

Acknowledgments

We gratefully appreciate the support from National Basic Research Program of China (2011CB933502) and the National Natural Science Foundation of China (21175065, 21375059, and 21335004) and the program B for outstanding Ph.D. candidates of Nanjing University.

References

[1] J.A. Cracknell, K.A. Vincent, F.A. Armstrong, Chem. Rev. 108 (2008) 2439–2461.
[2] M.J. Moehlenbrock, S.D. Minteer, Chem. Soc. Rev. 37 (2008) 1188–1196.
[3] Y. Zhang, M. Chu, L. Yang, Y. Tan, W. Deng, M. Ma, X. Su, Q. Xie, ACS Appl. Mater. Interfaces 6 (2014) 12808–12814.
[4] C. Agnes, M. Holzinger, A. Le Goff, B. Reuillard, K. Elouarzaki, S. Tingry, S. Cosnier, Energy Environ. Sci. 7 (2014) 1884–1888.
[5] V. Flexer, N. Brun, O. Courjean, R. Backov, N. Mano, Energy Environ. Sci. 4 (2011) 2097–2106.
[6] H. Sakai, T. Nakagawa, Y. Tokita, T. Hatazawa, T. Ikeda, S. Tsujimura, K. Kano, Energy Environ. Sci. 2 (2009) 133–138.
[7] K. MacVittie, J. Halamek, L. Halamkova, M. Southcott, W. D. Jemison, R. Lobeld, E. Katz, Energy Environ. Sci. 6 (2013) 81–86.
[8] T. Miyake, K. Haneda, N. Nagai, Y. Yatagawa, H. Onami, S. Yoshino, T. Abe, M. Nishizawa, Energy Environ. Sci. 4 (2011) 5008–5012.
[9] L. Halámková, J. Halámek, V. Bocharova, A. Szczupak, L. Alfonta, E. Katz, J. Am. Chem. Soc. 134 (2012) 5040–5043.
[10] T. Beneyton, I.P.M. Wijaya, C. Ben Salem, A.D. Griffiths, V. Taly, Chem. Commun. 49 (2013) 1094–1096.
[11] V. Andoralov, M. Falk, D.B. Suyatin, M. Granmo, J. Sotres, R. Ludwig, V.O. Popov, J. Schouenborg, Z. Blum, S. Shleev, Sci. Rep. 3 (2013) 1–11.
[12] A.N. Sekretaryova, V. Beni, M. Eriksson, A.A. Karyakin, A.P.F. Turner, M.Y. Vagin, Anal. Chem. 86 (2014) 9540–9547.
[13] E. Katz, A.F. Bückmann, I. Willner, J. Am. Chem. Soc. 123 (2001) 10752–10753.
[14] Z. Liu, B. Cho, T. Ouyang, B. Feldman, Anal. Chem. 84 (2012) 3403–3409.
[15] A. Zloczewska, A. Celebanska, K. Szot, D. Tomaszewska, M. Opallo, M. Jonsson-Niedziolka, Biosens. Bioelectron. 54 (2014) 455–461.
[16] M.N. Germain, R.L. Arechederra, S.D. Minteer, J. Am. Chem. Soc. 130 (2008) 15272–15273.
[17] L. Deng, C. Chen, M. Zhou, S. Guo, E. Wang, S. Dong, Anal. Chem. 82 (2010) 4283–4287.
[18] D. Wen, L. Deng, S. Guo, S. Dong, Anal. Chem. 83 (2011) 3968–3972.
[19] J. Cheng, Y. Han, L. Deng, S. Guo, Anal. Chem. 86 (2014) 11782–11788.
[20] F. Conzuelo, J. Vivekananthan, S. Pöller, J.M. Pingarrón, W. Schuhmann, ChemElectroChem 1 (2014) 1854–1858.
[21] Y. Wang, L. Ge, P. Wang, M. Yan, J. Yu, S. Ge, Chem. Commun. 50 (2014) 1947–1949.
[22] Z.L. Wang, Sci. Am. 298 (2008) 82–87.
[23] Z.L. Wang, W. Wu, Angew. Chem. Int. Ed. 51 (2012) 11700–11721.
[24] S. Wang, L. Lin, Z.L. Wang, Nano Energy 11 (2015) 436–462.
[25] R. Arechederra, S. Minteer, Anal. Bioanal. Chem. 400 (2011) 1605–1611.
[26] M. Zhou, J. Wang, Electroanalysis 24 (2012) 197–209.
[27] K.A. Foon, Blood 68 (1986) 1–31.
[28] T. Zheng, T. Tan, Q. Zhang, J.J. Fu, J.J. Wu, K. Zhang, J.J. Zhu, H. Wang, Nanoscale 5 (2013) 10360–10368.
[29] N. Chiorazzi, K.R. Rai, M. Ferrarini, N. Engl. J. Med. 352 (2005) 804–815.
[30] D.A. Novis, M. Walsh, D. Wilkinson, M. St. Louis, J. Ben-Ezra, Arch. Pathol. Lab. Med. 130 (2006) 596–601.
[31] R. Paredes-Aguilera, L. Romero-Guzman, N. Lopez-Santiago, L. Burbano-Ceron, C.-D. Monte, S. Nieto-Martinez, Am. J. Hematol. 68 (2001) 69–74.
[32] L. Belov, O. de la Vega, C.G. dos Remedios, S.P. Mulligan, R.I. Christopherson, Cancer Res. 61 (2001) 4483–4489.
[33] T. Flohr, A. Schrauder, G. Cazzaniga, R. Panzer-Grümayer, V. Van Der Velden, S. Fischer, M. Stanulla, G. Basso, F. Niggli, B. Schäfer, Leukemia 22 (2008) 771–782.
[34] R. Ghossein, S. Bhattacharya, Eur. J. Cancer 36 (2000) 1681–1694.
[35] T. Zheng, J.J. Fu, L. Hu, F. Qiu, M. Hu, J.J. Zhu, Z.C. Hua, H. Wang, Anal. Chem. 85 (2013) 5609–5616.
[36] W. Zhao, C.H. Cui, S. Bose, D. Guo, C. Shen, W.P. Wong, K. Halvorsen, O.C. Farokhzad, G.S.L. Teo, J.A. Phillips, D.M. Dorfman, R. Karnik, J.M. Karp, Proc. Natl. Acad. Sci. USA 109 (2012) 19626–19631.
[37] L. Qu, J. Xu, X. Tan, Z. Liu, L. Xu, R. Peng, ACS Appl. Mater. Interfaces 6 (2014) 7309–7315.
[38] J. Zhu, T. Nguyen, R. Pei, M. Stojanovic, Q. Lin, Lab Chip 12 (2012) 3504–3513.
[39] D. Shangguan, Y. Li, Z. Tang, Z.C. Cao, H.W. Chen, P. Mallikaratchy, K. Sefah, C.J. Yang, W. Tan, Proc. Natl. Acad. Sci. USA 103 (2006) 11838–11843.
[40] P.-P. Gai, C.-E. Zhao, Y. Wang, E.S. Abdel-Halim, J.-R. Zhang, J.-J. Zhu, Biosens. Bioelectron. 62 (2014) 170–176.
[41] O. Neumann, D. Zhang, F. Tam, S. Lal, P. Wittung-Stafshede, N.J. Halas, Anal. Chem. 81 (2009) 10002–10006.
[42] D. Shangguan, Z. Cao, L. Meng, P. Mallikaratchy, K. Sefah, H. Wang, Y. Li, W. Tan, J. Proteome Res. 7 (2008) 2133–2139.
[43] Y. Chen, Y. Li, D. Sun, D. Tian, J. Zhang, J.J. Zhu, J. Mater. Chem. 21 (2011) 7604–7611.
[44] C. Pan, M. Guo, Z. Nie, X. Xiao, S. Yao, Electroanalysis 21 (2009) 1321–1326.
[45] W. Li, J. Wang, J. Ren, X. Qu, Angew. Chem. Int. Ed. 52 (2013) 6726–6730.

Please cite this article as: P.-P. Gai, et al., Ultrasensitive self-powered cytosensor, Nano Energy (2015), http://dx.doi.org/10.1016/j.nanoen.2015.03.035